Research Article | Vol. 33, No. 15 / 28 Jul 2025 / Optics Express 30967
Optics EXPRESS

Broadband and wide-view cholesteric liquid crystal polarization selective reflectors

YUQIANG DING,[†] YEFU ZHANG,[†] YUGE HUANG, YONGZIYAN MA, ZHENYI LUO, PO-SHENG CHIU, AND SHIN-TSON WU[*]

College of Optics and Photonics, University of Central Florida, Orlando, FL 32816, USA
[†]These authors contributed equally
[*]*swu@creol.ucf.edu*

Abstract: The Bragg reflection of a cholesteric liquid crystal (CLC) gradually turns into phase retardation effect as the incident angle increases, which causes the polarization degradation in the CLC medium and explains why it is challenging to achieve a broadband response over a wide viewing angle. In this paper, we propose three novel solutions to address this issue, including a newly designed helicoidal structure, using a biaxial LC material, and laminating a compensation film to the CLC layer. All the results presented in this work are based on theoretical analysis and numerical simulations. By studying the polarization behavior and the eigenstates of the structures, we reveal the underlying principles behind the broadband, wide-view performance. Through optimization, our proposed methods can achieve nearly 100% reflectance across the visible spectrum up to ±45° incident angle, while keeping a decent contrast ratio. These findings offer new insights for realizing broadband and wide-view CLCs for display applications.

© 2025 Optica Publishing Group under the terms of the Optica Open Access Publishing Agreement

1. Introduction

Cholesteric liquid crystals (CLCs) are a class of photonic materials widely studied for their unique helical structures and polarization-selective optical properties [1–4]. As a one-dimensional periodic material, CLCs exhibit a helical molecular distribution, with the helix axis perpendicular to the LC director and a pitch typically on the order of hundreds of nanometers. This periodic modulation of the refractive index gives rise to distinctive optical behavior, particularly the formation of wavelength-selective reflection bands. Within these bands, CLCs exhibit strong Bragg reflection for the circularly polarized light with the same handedness as the helix, while transmitting the opposite polarization. The central wavelength (λ_o) and bandwidth ($\Delta\lambda$) of this reflection band are determined by the pitch length (p), birefringence (Δn), and incident angle. Several simulation methods, such as the 4×4 matrix method [5] and rigorous coupled-wave analysis (RCWA) [6,7], have been widely used to analyze the spectral and angular responses of CLCs.

Because of the inherent polarization selectivity, CLCs have found widespread applications in optical devices, including pancake optics for virtual reality (VR) [8,9], light recycling films for displays, sunlight readable reflective displays, and broadband polarizers. However, a conventional single-layer CLC with a fixed pitch exhibits a relatively narrow reflection band ($p\Delta n$) and cannot achieve broadband operation across the entire visible spectrum. This limitation significantly hinders its potential in full-color and wide-angle display applications. Moreover, due to the blue shift of Bragg reflection at an oblique incident angle, the CLC must provide an extended reflection range, especially at the longer wavelength side, to maintain consistent performance under oblique viewing conditions. To address this issue, pitch modulation strategies have been proposed, including discrete multilayer structures [10] and gradient-pitch configurations [11–13]. These approaches leverage nonuniform pitch distributions to broaden the reflection bandwidth and have shown promising results.

#569217
Journal © 2025
https://doi.org/10.1364/OE.569217
Received 28 May 2025; revised 1 Jul 2025; accepted 3 Jul 2025; published 14 Jul 2025

Despite these advancements, our recent analysis revealed a fundamental limitation in conventional CLC designs, that is a broadband and high-efficiency wide-view reflector cannot be realized solely through pitch modulation [14]. More specifically, as the incident angle deviates from the helical axis, the eigenstates of light polarization shift from circular to linear polarization, a phenomenon called polarization conversion effect [15,16]. This effect leads to polarization degradation and a significant drop in contrast ratio at large incident angles (over 30°), undermining the performance of CLC-based optical components [17,18].

In this paper, to address this challenge we investigate multiple strategies aimed at mitigating the polarization degradation induced by the polarization conversion effect. Specifically, we explore novel CLC structure designs, biaxial LC materials, and phase compensation techniques. By either eliminating the polarization conversion or compensating for its effects, we demonstrate that a broadband, wide-view CLC reflector with high contrast ratio can be achieved. This work provides new insights into the design of next-generation CLC materials and structures, offering guidance for their integration into near-eye display systems.

2. Polarization conversion of a planar CLC

In a conventional CLC structure, also known as planar CLC, the helix axis is perpendicular to the local LC director. The LC molecules form layers in which the directors are aligned uniformly. Across these layers, the LC directors rotate, creating a sinusoidal helical pattern along the helix axis, as illustrated in Fig. 1(a). Such CLCs strongly reflect light with a specific circular polarization. At normal incidence, this polarization selectivity is highly effective, and the transmitted light remains circularly polarized after passing through the CLC layer. However, at oblique incident angles and outside the reflection band, the transmitted light no longer maintains an ideal circular polarization, as Fig. 1(b) depicts. To demonstrate this polarization conversion effect more clearly, we use a multilayer CLC configuration, whose structure is shown in Fig. 1(c). All the incident angles (θ) mentioned in this paper refer to the angle of incidence in air, measured relative to the surface normal before the light enters the glass substrate. In our simulations, the glass substrate has a refractive index of 1.6. Figure 1(d) shows the reflection spectra of the multilayer CLC at incident angles = 0° and 30°. The pitches of the layers are 293.75 *nm*, 325 *nm*, 356.25 *nm*, 387.5 *nm*, and 418.75 *nm*, with each layer having a thickness of 5 μm. The refractive indices of the LC material are n_e = 1.7 and n_o = 1.5. At = 30°, the reflection efficiency corresponding to the first layer (p = 293.75 *nm*) is nearly ideal. However, as the light traverses through the CLC medium, the reflection efficiency drops due to polarization degradation. In our recent study, we thoroughly examined the eigenstates of CLCs at different incident angles [14]. The polarization of these eigenstates gradually changes from circular to linear as the incident angle deviates from the helical axis. At large incident angles, the eigenstates exhibit elliptical polarization. Therefore, in theory, it is challenging to achieve a high-contrast, broadband, wide-view reflector using multi-layer or gradient planar CLCs alone [10,11]. This conventional structure can offer broadband performance only at near normal incidence.

In the following, we describe three approaches to address the polarization degradation problem and enhance the CLC reflectance in the visible spectral range with incident angle varying from 0^o to 60^o.

3. Broadband wide-view CLC with tilted helicoidal structures

To better understand the polarization degradation in a planar CLC, it is important to first look into the basic optical properties of LC materials. One key factor is birefringence, which is the difference between the extraordinary and ordinary refractive indices. In general, higher birefringence causes the polarization state of light to change more rapidly as it travels through the material, especially in a thicker layer. In addition, when the light enters at a larger angle,

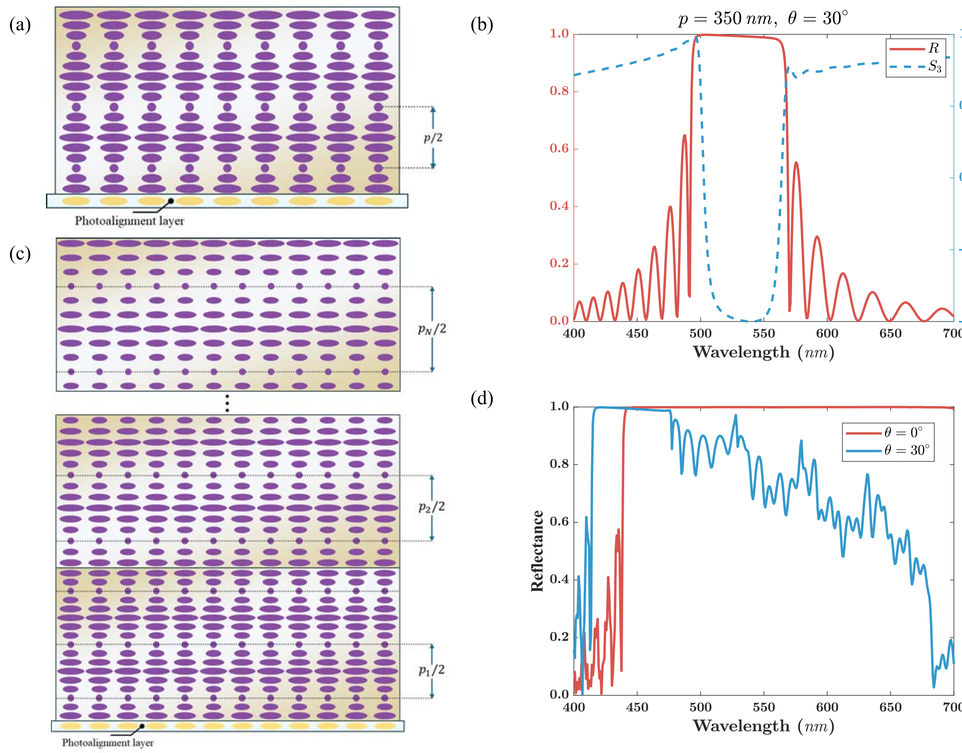

Fig. 1. (a) Schematic of a planar CLC structure. (b) Wavelength-dependent reflectance and transmitted light polarization (represented by the Stokes parameter S_3) for a CLC with a 350 nm pitch at 30° incident angle. (c) Schematic of a multilayer CLC structure with varying pitches. (d) Simulated reflectance spectra at various incident angles for the multilayer CLC configuration.

it becomes more sensitive to the birefringence. As a result, the circular polarization begins to break down gradually, particularly at oblique incidence.

To mitigate this issue, one effective approach is to reduce the birefringence of the employed LC material. In our work, we achieve this by modifying the LC alignment. Specifically, we tilt the orientation of the planar nematic LC and then introduce a rotational twist, creating a new helicoidal CLC structure [19,20], as shown in Fig. 2(a). In this configuration, when light enters at an oblique angle, the effective refractive index along the z-direction increases, which leads to a reduction in overall birefringence. As a result, the phase retardation is also reduced. This structural change introduces an extra degree of control over the molecular alignment, which significantly affects how light interacts with the LC layer. From the perspective of polarization eigenstates, we also analyze the behavior of the modified helicoidal structure. The results show that the new design enhances the effective refractive index along the z-direction, which helps maintain polarization stability and keeps the eigenstates closer to circular polarization, even at larger incident angles.

As shown in our recent study, no analytical solution exists for describing the eigenstates under tilted incidence. Therefore, we evaluate the polarization conversions using the Stokes parameter S_3, which characterizes the degree of circular polarization. Figure 2(b) shows that under normal incidence, the output polarization in a planar CLC oscillates around the circular state as the LC thickness increases. However, at larger incident angles, the oscillation amplitude

Optics EXPRESS

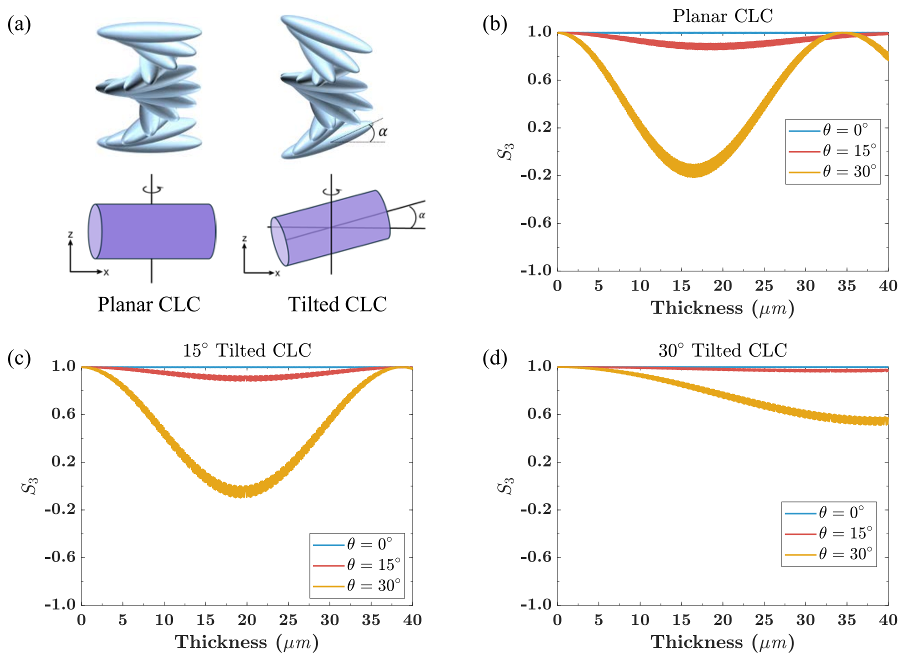

Fig. 2. (a) Schematic comparison between planar and tilted helicoidal CLC structures. (b) Polarization conversion (Stokes parameter S_3) versus thickness for planar CLCs with a 300-nm pitch, under various incident angles. (c) Polarization conversion versus thickness for 15° tilted helicoidal CLCs with a 300-nm pitch. (d) Polarization conversion versus thickness for 30° tilted helicoidal CLCs with a 300-nm pitch. The wavelength is fixed at λ=550 nm in both (b), (c) and (d).

increases significantly, indicating a stronger deviation from circular polarization and a shift of the eigenstates toward linear polarization. When a helicoidal CLC structure with a tilt angle of 15° is used, the polarization oscillation is slightly reduced, as Fig. 2(c) depicts. As the tilt angle increases to 30°, the oscillation is significantly suppressed. Figure 2(d) shows that the polarization state stays much closer to circular, even at oblique incidence. In other words, the eigenstates remain nearly circular under these conditions, confirming the effectiveness of the structural modification in maintaining polarization stability.

It is important to note, however, that reducing birefringence comes with a trade-off. Specifically, it leads to a narrower reflection bandwidth [21]. Therefore, to fully benefit from improved polarization stability while still maintaining adequate spectral performance, an optimization process is required to balance these competing factors. Besides, a high Δn LC material helps solve this problem.

After establishing the design principle of the modified structure, optimization is conducted to achieve the best possible optical performance. The goal of this optimization is to realize a high contrast ratio across the visible spectral range ($400 - 700$ nm) while maintaining good performance over a wide range of incident angles. The refractive indices of the LC material remain $n_e = 1.7$ and $n_o = 1.5$ throughout the process. To accommodate practical fabrication constraints for tilted CLC structures, a gradient pitch profile is introduced. Specifically, the pitch varies exponentially along the z-direction, which enables smoother structural conversions and improved optical behavior. The detailed fabrication guidance will be described on Sec. 5. The variables considered during optimization include the initial pitch p_i, the final pitch p_f, the total cell gap d, and the tilt angle α. Figures 3(a-b) show the optimized results, demonstrating strong angular and spectral responses. Across the target wavelength and angle ranges (0°−30°), the reflectance remains close to 100%, indicating excellent performance. As the incident angle increases, the blue shift becomes more obvious, and the efficiency gradually drops. To further quantify the effectiveness of the design, a typical red (R = 633 nm), green (G = 527 nm) and blue (B = 464.5 nm) LED spectrum (Fig. 3(c)) is used to calculate the contrast ratio (CR) using the following equation:

$$CR = \frac{\int R(\lambda)S(\lambda)d\lambda}{\int T(\lambda)S(\lambda)d\lambda}, \tag{1}$$

where $R(\lambda)$ is the reflectance, $T(\lambda)$ is the transmittance, and $S(\lambda)$ is the normalized LED spectral intensity. Based on the reflectance data shown in Fig. 3(a), the calculated CR is 593 : 1, 795 : 1, and 903 : 1 at = 0°, 15°, and 30°, respectively. At = 45°, the CR drops to 163 : 1. As the incident angle continues to increase to = 60°, the edge of the reflection band shifts to ~650 nm and the efficiency drops slightly to ~95%. Although the target is set at 30°, the CLC still works reasonably well at larger incident angles, with a reduced contrast ratio. These results highlight the structure's effectiveness in delivering high contrast and wide-angle performance within the visible spectral range.

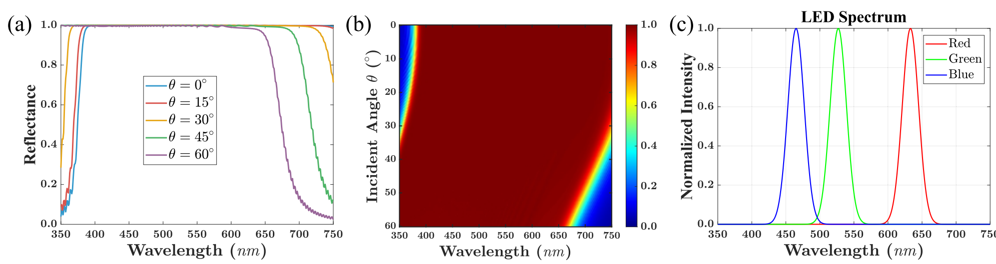

Fig. 3. (a) Reflectance spectra of helicoidal CLCs as a function of wavelength at different incident angles. (b) Angular and spectral reflectance response of helicoidal CLCs. (c) Normalized emission spectra of RGB LEDs. In (a) and (b), the CLC pitch varies exponentially from $p_i = 495$ nm to $p_f = 248$ nm, with a total cell thickness $d = 50.03$ μm and a tilt angle $\alpha = 33.6°$.

4. Broadband wide-view CLC with biaxial material and compensation film

After demonstrating the feasibility of structural modification, two additional methods to improve the polarization performance of CLCs are introduced in this section. Based on our previous analysis, increasing the effective refractive index along the z-direction reduces polarization conversions and shifts the eigenstates of the CLC closer to circular polarization. This insight provides a clear design direction for improving the broadband spectral stability over a wide-view angle.

4.1. Biaxial liquid crystal for broadband and wide-angle reflection

From the material perspective, one promising method is to use a biaxial LC, as illustrated in Fig. 4(a). Unlike uniaxial LCs, which have two principal refractive indices, biaxial LCs possess three distinct indices n_x, n_y, and n_z. By carefully choosing a biaxial LC where n_z lies between n_x and n_y, we can effectively enhance the refractive index along the propagation (z) direction. This mimics the optical behavior of a helicoidal CLC structure, but within a fully planar configuration [22,23].

The biaxial CLC structure maintains a planar alignment while introducing a multilayer pitch distribution. In the optimization process, the refractive index along the z-direction, n_z, is treated

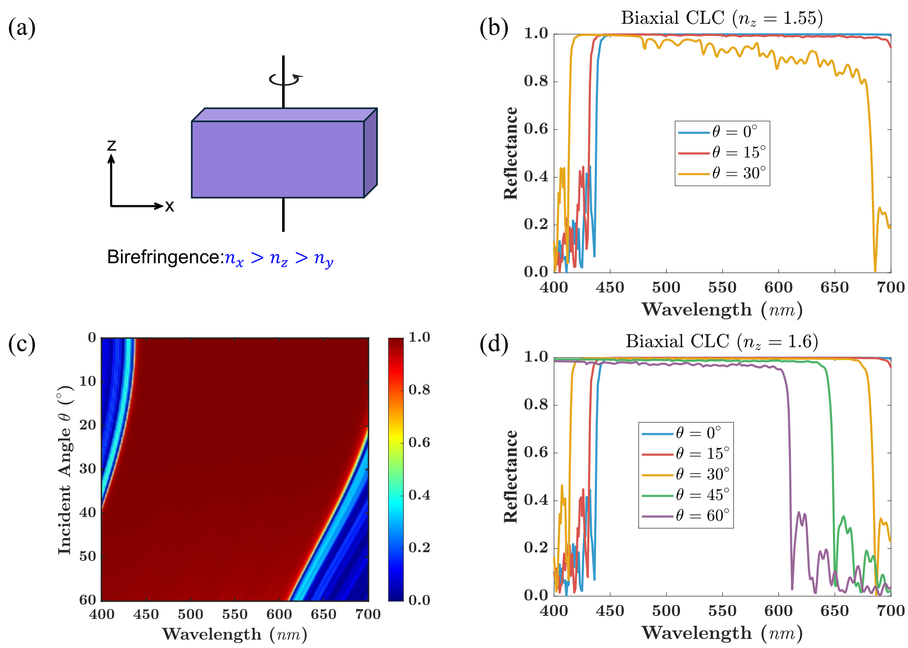

Fig. 4. (a) Schematic illustration of a biaxial CLC structure. (b) Reflectance as a function of wavelength at different incident angles for the biaxial CLC with $n_z = 1.55$. (c) Angular and spectral reflectance response for biaxial CLCs with $n_z = 1.6$. (d) Reflectance as a function of wavelength at different incident angles for the biaxial CLC with $n_z = 1.6$. The pitches used in (b), (c) and (d) are 293.75 nm, 325 nm, 356.25 nm, 387.5 nm, and 418.75 nm, with each layer having a thickness equal to 12 times its pitch.

as a variable. As n_z increases, the optical performance begins to resemble that of a helicoidal CLC with a larger tilt angle, which means that the increase of n_z suppresses the phase degradation. Figure 1(d) illustrates the reflectance performance for $n_z = 1.5$. The pitches used in Fig. 4(b-d) are 293.75 nm, 325 nm, 356.25 nm, 387.5 nm, and 418.75 nm, with each layer having a thickness equal to 12 times its pitch. As shown in Fig. 4(b), increasing n_z leads to higher reflectance, but it still does not reach an ideal level. After optimization, the best-performing material configuration is found to have $n_x = 1.7$, $n_y = 1.5$ and $n_z = 1.6$. The simulation results, presented in Fig. 4(c-d), show that the reflectance stays close to 100% across a wide portion of the visible spectrum, particularly from 450 nm to 650 nm. We obtain excellent broadband and wide-view performance across the $0°-30°$ incidence angle range. Notably, even at θ=30°, the minimum reflectance within the target bandwidth remains as high as 99.42%, indicating strong polarization retention and minimal degradation. Moreover, the contrast ratio at = 30° still exceeds 170:1, highlighting the effectiveness of biaxial material design in preserving high optical performance across angles. As shown in Fig. 4(d), the simulated results at = 45° and 60° are also included for comparison, showing a slight drop in reflectance and blue shift. These results are less impressive than those shown in Fig. 3 for the helicoidal structure.

In summary, the use of a biaxial LC provides a material-based solution to polarization degradation by increasing the z-direction refractive index and stabilizing the polarization state. When combined with multilayer pitch design, this method shows strong potential for use in advanced wide-view optical devices.

Optics EXPRESS

4.2. Compensation film design for polarization correction

In addition to structural and material modifications, another straightforward and practical method to improve the polarization performance of a planar CLC is to use a compensation film. This approach aims to compensate for the polarization degradation that occurs due to the intrinsic birefringence of the CLC layer, especially at larger incident angles.

To understand the compensation principle, let us consider a planar CLC structure with a small pitch. In such cases, the rotation of LC directors along the z-direction is very rapid, leading to a strong anisotropic optical response. This behavior is similar to that of a negative C-plate [24], as illustrated in Fig. 5(a). Under normal incidence, the effective extraordinary refractive index is primarily determined by the optical axis orientation and the intrinsic properties of the CLC. Thus, the entire CLC layer can be approximated as functioning like a negative uniaxial film. To evaluate the polarization behavior and the feasibility of compensation, we analyze the phase retardation characteristics using S_3 parameter. Figure 5(c) compares the behavior of a planar CLC and an ideal negative C-plate. In this plot, the red region denotes the reflection band of the CLC whose right side is the corresponding polarization needed compensation. While the blue region represents the phase conversion behavior of the CLC begins to closely match that of the negative C-plate (starting around 530 nm). Such a similarity implies that this spectral region is suitable for optical compensation.

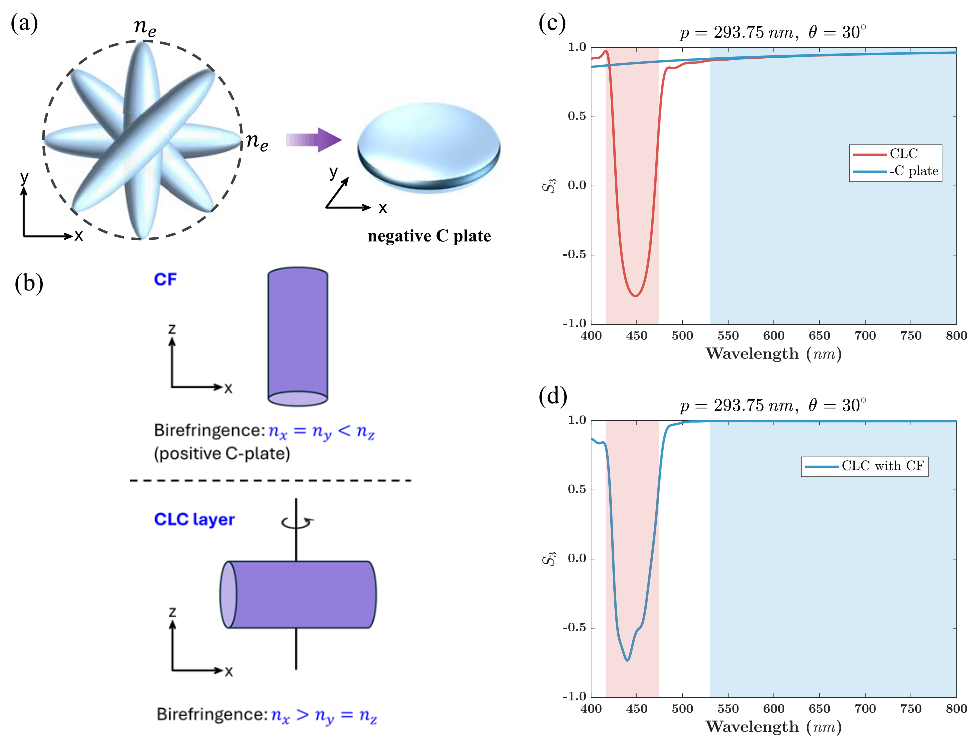

Fig. 5. (a) Comparison between a planar CLC structure (top view) and a negative C-plate (oblique top view). (b) Schematic of a CLC layer combined with a compensation film. (c) Stokes parameter S_3 as a function of wavelength for both the CLC and the negative C-plate. (d) Stokes parameter S_3 as a function of wavelength for the CLC structure with a positive C-plate compensation film (CF).

Based on this match, a positive C-plate is introduced on top of the CLC medium to form a compensation stack, as shown in Fig. 5(b). The positive C-plate induces a phase retardation

Optics EXPRESS

opposite that of the CLC in the degradation region. As a result, the polarization distortion introduced by the CLC can be partially compensated, improving the polarization purity of the transmitted light. This effect is most noticeable in the wavelength region beyond 600 nm, where the match in phase behavior is the strongest.

However, it is important to note that there is a mismatch region between the red and blue regions in Fig. 5(c). In this gap, the phase behavior of the CLC changes rapidly, and the compensation effect becomes ineffective due to the lack of phase matching. The sharp conversion at the edge of the reflection band makes this region particularly difficult to compensate. Within this mismatch region, the positive C-plate does not effectively correct the polarization distortion, resulting in residual polarization errors and decreased optical efficiency. This phenomenon is clearly observed in Fig. 5(d), which shows the transmitted S_3 parameter of the CLC with the compensation film applied. Beyond 530 *nm*, the transmitted light exhibits a polarization state that remains close to circular, confirming the effectiveness of the compensation. However, as the wavelength approaches the main reflection band, the polarization begins to deviate from the ideal state, indicating the breakdown of the compensation effect in that range. Therefore, to ensure optimal performance, it is necessary to avoid using light within this mismatch region. In practice, the spectral output of the light source should be filtered or limited to exclude the compensation bandgap to maintain high polarization fidelity across the operating range.

With the addition of a compensation film, CLC structures can be designed to reflect multiple discrete spectral bands, specifically narrow RGB bands, rather than a continuous broadband range. This narrowband approach is motivated by the sharp spectral transition at the edge of the CLC reflection band, which makes it challenging to align multiple bands precisely within the visible range. To better align the reflection peaks with the RGB wavelengths, the LC birefringence should be reduced, which in turn narrows the reflection bandwidth. This strategy not only helps avoid the problematic wavelength regions near the bandgap edges but also allows for more precise control over polarization behavior in each color channel. Such narrowband multi-reflection designs are especially advantageous in applications like full-color reflective displays, AR systems, and polarization-sensitive imaging, where maintaining distinct polarization states across RGB channels is essential for performance and image quality.

5. Discussion

Due to the intrinsic helical structure of CLCs, polarization conversions occur as light propagates through the material, making broadband reflection difficult to achieve. One effective way to reduce this effect is by increasing the refractive index along the z-direction, which helps maintain circular polarization, especially at oblique angles. This study explored two approaches based on this principle: a novel helicoidal CLC structure and the use of biaxial LC materials. Both methods demonstrated near-unity broadband reflectance and high contrast ratios across wide viewing angles. Additionally, a compensation film using a positive C-plate was introduced to counteract polarization rotation in planar CLCs. While small-pitch CLCs can be approximated as negative C-plates and partially compensated, spectral mismatch near the reflection band edge limits full polarization recovery and will slightly reduce efficiency.

This study primarily focuses on methods for achieving broadband reflection in CLC-based devices and provides detailed theoretical analysis and simulation results to support each approach. In addition, practical fabrication guidance for realizing the helicoidal structure is presented. The first fabrication method involves preparing an LC cell filled with a mixture of LC material, chiral dopant, and UV-sensitive dye. The chiral agent induces helical structure, while the UV dye enables spatial control of polymerization. During the curing process, UV light with a gradient intensity profile is applied along the incident direction. This results in a nonuniform polymerization rate, forming a gradient pitch structure throughout the cell. After curing, applying an external voltage tilts the CLC molecules, forming the desired helicoidal configuration. Another effective approach is to use polymer-stabilized CLCs [25–29], which are well-suited for forming stable gradient structures. In this process, the mixture includes a monomer, chiral dopant, and UV dye. Unlike the first method, the curing process here involves simultaneous application of UV light and voltage. The gradient light intensity induces a varying polymerization rate along the z-axis, resulting in a spatial gradient of polymer concentration. This structure remains fixed after curing and can function either passively or with an applied voltage for switchable applications.

As demonstrated in Sec. 3, the optimized CLC structure requires a relatively thick film to cover the full visible spectrum from 400 nm to 700 nm when using a low Δn LC material. However, for LC polymer systems with a higher birefringence (e.g., Δn>0.4) (from Merck), the same broadband performance can be achieved with a significantly thinner film. This makes the approach more practical and suitable for modern fabrication techniques.

6. Conclusion

In conclusion, we present three effective strategies to suppress the polarization conversion in a CLC system. These methods significantly improve the optical performance of a broadband and wide-view CLC. Through physical analysis, including eigenstate evaluation and angular and spectral response modeling, we demonstrate why these techniques work and how they influence polarization behavior. Reflectance within the target bandwidth can reach nearly 100%, accompanied by high contrast ratios. Collectively, these findings provide new insights into enhancing CLC performance and offer promising directions for future development in advanced optical and display technologies.

Funding. Meta Research.

Acknowledgments. The UCF group is indebted to Meta Platforms for partial financial support.

Disclosures. The authors declare no conflicts of interest.

Data Availability. Data underlying the results presented in this paper are not publicly available at this time but may be obtained from the authors upon reasonable request.

References

1. D. W. Berreman and T. J. Scheffer, "Bragg reflection of light from single-domain cholesteric liquid-crystal films," Phys. Rev. Lett. **25**(9), 577–581 (1970).
2. H. De Vries, "Rotatory power and other optical properties of certain liquid crystals," Acta Crystallogr. **4**(3), 219–226 (1951).
3. R. Dreher, G. Meier, and A. Saupe, "Selective Reflection by Cholesteric Liquid Crystals," Mol. Cryst. Liq. Cryst. **13**(1), 17–26 (1971).
4. Q. Hong, T. X. Wu, and S.-T. Wu, "Optical wave propagation in a cholesteric liquid crystal using the finite element method," Liq. Cryst. **30**(3), 367–375 (2003).
5. D. W. Berreman, "Optics in Stratified and Anisotropic Media: 4×4-Matrix Formulation," J. Opt. Soc. Am. **62**(4), 502–510 (1972).
6. M. G. Moharam and T. K. Gaylord, "Rigorous coupled-wave analysis of planar-grating diffraction," J. Opt. Soc. Am. **71**(7), 811–818 (1981).
7. J. Xiong and S.-T. Wu, "Rigorous coupled-wave analysis of liquid crystal polarization gratings," Opt. Express **28**(24), 35960–35971 (2020).
8. Z. Luo, Y. Ding, Q. Yang, *et al.*, "Ghost image analysis for pancake virtual reality systems," Opt. Express **32**(10), 17211–17219 (2024).
9. Y. Ding, Z. Luo, G. Borjigin, *et al.*, "High-efficiency and ultracompact pancake optics for virtual reality," J. Soc. Inf. Disp. **32**(5), 341–349 (2024).
10. H. Choi, J. Kim, S. Nishimura, *et al.*, "Broadband Cavity-Mode Lasing from Dye-Doped Nematic Liquid Crystals Sandwiched by Broadband Cholesteric Liquid Crystal Bragg Reflectors," Adv. Mater. **22**(24), 2680–2684 (2010).
11. C. Binet, M. Mitov, and M. Mauzac, "Switchable broadband light reflection in polymer-stabilized cholesteric liquid crystals," J. Appl. Phys. **90**(4), 1730–1734 (2001).
12. X. Chen, L. Wang, Y. Chen, *et al.*, "Broadband reflection of polymer-stabilized chiral nematic liquid crystals induced by a chiral azobenzene compound," Chem. Commun. **50**(6), 691–694 (2014).
13. D. J. Broer, J. Lub, and G. N. Mol, "Wide-band reflective polarizers from cholesteric polymer networks with a pitch gradient," Nature **378**(6556), 467–469 (1995).

Optics EXPRESS

14. Y. Ding, Y. Zhang, Y. Ma, *et al.*, "Polarization conversion effect in cholesteric liquid crystal-based polarization volume gratings," Opt. Express **32**(25), 44425–44436 (2024).
15. V. A. Belyakov, V. E. Dmitrienko, and V. P. Orlov, "Optics of cholesteric liquid crystals," Sov. Phys. Usp. **22**(2), 64–88 (1979).
16. E. Kats, "Optical properties of cholesteric liquid crystals," Sov. Phys. JETP **32**(5), 1004–1007 (1971).
17. Y. Ding, Y. Gu, Q. Yang, *et al.*, "Breaking the in-coupling efficiency limit in waveguide-based AR displays with polarization volume gratings," Light:Sci. Appl. **13**(1), 185 (2024).
18. Y. Huang, L. Lu, N. Diorio, *et al.*, "60-3: *Invited Paper:* Liquid Crystal Optics for AR/VR/MR Near Eye Displays," Dig. Tech. Pap. - Soc. Inf. Disp. Int. Symp. **54**(1), 857–860 (2023).
19. V. S. Sutormin, I. V. Timofeev, M. N. Krakhalev, *et al.*, "Orientational transition in the cholesteric layer induced by electrically controlled ionic modification of the surface anchoring," Liq. Cryst. **44**(3), 484–489 (2017).
20. H. Schmiedel, R. Stannarius, C. Cramer, *et al.*, "Induction of Tilted Cholesteric Structures in Microconfined Liquid Crystals," Mol. Cryst. Liq. Cryst. **262**(1), 167–178 (1995).
21. R. Ozaki, "Simple model for estimating band edge wavelengths of selective reflection from cholesteric liquid crystals for oblique incidence," Phys. Rev. E **100**(1), 012708 (2019).
22. H. Ogawa, E. Stibal-Fischer, and H. Finkelmann, "Cholesteric Liquid-Crystalline Side-on Polysiloxanes: Effects of Biaxiality on the Cholesteric Structure," Macro Chemistry & Physics **205**(5), 593–599 (2004).
23. R. G. Priest and T. Lubensky, "Biaxial model of cholesteric liquid crystals," Phys. Rev. A **9**(2), 893–898 (1974).
24. S. Nishimura and H. Mazaki, "Viewing angle compensation of various LCD modes by using a liquid crystalline polymer film Nisseki LC film," Liquid Crystals X. Edited by I-C. Khoo, Proc. SPIE **6332**, 633203 (2006).
25. D.-K. Yang, L.-C. Chien, and J. W. Doane, "Cholesteric liquid crystal/polymer dispersion for haze-free light shutters," Appl. Phys. Lett. **60**(25), 3102–3104 (1992).
26. M. Mitov, "Cholesteric Liquid Crystals with a Broad Light Reflection Band," Adv. Mater. **24**(47), 6260–6276 (2012).
27. T. J. White and D. J. Broer, "Programmable and adaptive mechanics with liquid crystal polymer networks and elastomers," Nat. Mater. **14**(11), 1087–1098 (2015).
28. H. Zhou, H. Wang, W. He, *et al.*, "Research Progress of Cholesteric Liquid Crystals with Broadband Reflection," Molecules **27**(14), 4427 (2022).
29. K. M. Herbert, H. E. Fowler, J. M. McCracken, *et al.*, "Synthesis and alignment of liquid crystalline elastomers," Nat. Rev. Mater. **7**(1), 23–38 (2021).